ICRC 2001

Simulation study of the CALET instrument at the Japanese experiment module on International Space Station

K. Yoshida[1], S. Torii[1], T. Tamura[1], K. Hibino[1], J. Nishimura[2], T. Yamagami[2], H. Murakami[3], and K. Kasahara[4]

[1]Faculty of Engineering, Kanagawa University, Yokohama 221-8686, Japan

[2]The Institute of Space and Astronautical Science, Sagamihara 229-8510, Japan

[3]Department of Physics, Rikkyo University, Tokyo 171-8510, Japan

[4]Department of Electronic Information Systems, Shibaura Institute of Technology, Omiya 330-8570, Japan

Abstract. We have carried out simulation study on the CALET (CALorimetric Electron Telescope) instrument, especially for heavy payload, to optimize the performance for electron measurement up to 10 TeV. The CALET for heavy payload consists of a sampling imaging calorimeter brought from the balloon-borne electron telescope with scintillating fibers (BETS) and a total absorption calorimeter with BGO log arrays. By the analysis of the simulated events, we have confirmed the performance of the CALET as follows. The proton rejection power is as much as 10^6 with the BGO thickness of 35 cm (32 r.l.). The energy resolution is estimated to be $30\%/\sqrt{E(\text{GeV})}$ and the incident angle is determined by the imaging with an angular resolution less than 1 deg.

1 Introduction

The design of the CALET (CALorimetric Electron Telescope) instrument has two concepts proposed for the observation of TeV electrons at the Japanese Experiment Module Exposure Facility (JEM/EF) on the International Space Station (ISS). One design has the weight of 500 kg for the standard payload and the other has the weight of 2,500 kg for the heavy payload. The baseline detector for the standard payload is brought from the balloon-borne electron telescope with scintillating fibers (BETS) (Torii *et al.* (2001a), Tamura *et al.* (2000)). In order to get an additional rejection power of a magnitude of 2, the detector for the heavy payload is composed of the BETS-type imaging calorimeter and the total absorption calorimeter with BGO log arrays. The mission concepts and scientific objects are described in Torii *et al.* (2001b).

In order to observe electrons up to 10 TeV, it is required to achieve a rejection power of $\sim 10^6$. For this purpose, we are considering to put a total absorption calorimeter under an imaging calorimeter similar to the standard payload. Sum-

marizing briefly the detector, the sampling imaging calorimeter is stacks of 70cm×70cm planar scintillating fiber detector arrays with a 1.0 mm square cross section aligned in X and Y directions, interleaved with lead plates. The total thickness of lead plates is 13 radiation lengths (r.l.). The total absorption calorimeter consists of 2.5cm×2.5cm×35cm BGO logs which are placed aligned in X and Y directions layer by layer and the thickness is 32 r.l. The total thickness is 45 r.l. and 2.1 nuclear mean free path for protons. From this design, it is possible to measure the full shower development of electrons up to 10 TeV and to detect a considerable part of secondary hadrons produced by the nuclear interactions of protons.

In this paper we present the simulated performance of the CALET, especially for heavy payload design, which has a capability to observe cosmic ray electrons in the energy range from several GeV to 10 TeV. We also report about the performance for measuring the gamma-rays from 1 GeV to 1 TeV.

2 Simulation System

The simulation model detector is slightly different from the above configuration. In order to optimize the thickness of the BGO log arrays with enough rejection power, the thickness is arranged in 50 cm larger than that of the above. All other configurations except for this are same as the design of heavy payload (Torii *et al.* (2001b)).

As an electron enters the instrument, electro-magnetic cascade shower ensues in the lead plates and BGO logs. The shower is imaged in three dimensions by the scintillating fiber arrays and attenuated by the BGO log arrays. The direction of the electron is measured by the fiber images and the energy is measured by the fiber and BGO arrays.

Monte Carlo Simulations were performed by using the EPICS code developed by one of the authors (Kasahara (2001)). EPICS is Electron-Photon Induced Cascade Simulator in a detector and can also deal with hadrons and photoproduction of hadrons. In this code, the results of electro-

magnetic process has been compared with a major simulation code, GEANT, and the reliability is completely proven. The hadronic interaction model without target fragmentation was simulated by Nucrin/Hadrin model at $E < 5$ GeV, Fritiof v1.6 model at $5 \leq E < 500$ GeV, and the phenomenological ad-hoc model at $E \geq 500$ GeV. The ad-hoc model is fitted to accelerator data including SPS UA5 data, which is developed for simulation code COSMOS by K.Kasahara (Kasahara (2001) and references therein). The simulation results were also compared with the beam tests of BETS(Tamura *et al.* (2000),Torii *et al.* (2000)).

EPICS simulation system provides to propagate particles through a model of the instrument, accumulating energy deposits. The simulation model incorporates many fine details of the instrument, including individual scintillating fibers, lead plates, and BGO logs, though readout hardware and electronics are not simulated. Instead of readout hardware and electronics, the energy deposits in the individual scintillating fibers and BGO logs are recorded. In this simulation, the Landau-Vavilov-Gaussian fluctuation of energy loss is considered. As a minimum ionizing particle is detected in the scintillating fiber arrays, electron and gamma-rays are identified with the imaging capability. The treated minimum kinetic energy of electrons, gamma rays, and heavy particles ($\mu, \pi, K, p, ...$) is 100 keV.

Recorded data from the events are analyzed to determine the scientific performance of the instrument, such as angular resolution, energy resolution, and proton rejection power.

3 Simulated Results of Performance

The simulation system described above has been used to generate event data for electrons, protons and gamma-rays. Below, we describe instrument performance parameters derived from these event data.

3.1 Proton Rejection

Average lateral spread of an electro-magnetic shower in lead is roughly estimated at ∼1.6 cm (one Moliere unit). On the other hand the proton induced shower should have a wide spread due to the spread of secondary pions in the nuclear interactions. This difference is clearly observed in the images of scintillating fibers. As for the BETS, as the method for electron selection by the imaging analysis we have used the ratio of energy deposition within 5 mm from the shower axis to the total (RE) for the events of electrons and protons. However, at higher energies than 100 GeV the proton induced shower has a narrower spread and increases the ratio of energy. Therefore it is more difficult to reject proton events in higher energies than 100 GeV only with the RE selection. By using neural network analysis of the images, for example, proton rejection power is estimated to be ∼ 10^4 (Zhang (1998)). To obtain an additional proton rejection power for the electron observation up to 10 TeV, the total absorption calorimeter of BGO log arrays is needed.

We generated electrons with an energy of 0.1 TeV, 1 TeV, and 10 TeV at the center of top of detector with the vertical direction. Protons with an energy three times larger than the electrons, which have similar shower energy with the electrons, are compared as the background of electrons. Simulated number of electron events is 1×10^3 for 0.1 TeV, 1 TeV and 10 TeV. The number of protons is 1×10^5 for 0.3 TeV, 3 TeV and 30 TeV. Figure 1 shows examples of the reconstructed images of scintillating fibers and BGO logs with X and Y directions for 10 TeV electron and 30 TeV proton in the vertical direction.
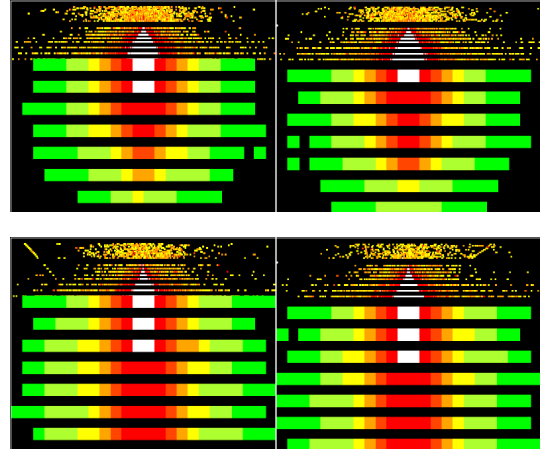
Fig. 1. Examples of the reconstructed images of scintillating fiber and BGO log arrays with X and Y directions. The upper is a electron-induced shower of 10 TeV and the lower is a proton-induced shower of 30 TeV. The size is 60cm×50cm in one direction. The energy deposits in each image are presented by gray scale. The fine points in each image show the energy deposits in the fibers and the coarse squares, corresponding to a 2.5 cm cross-section, show the deposits in BGO logs.

We selected electron events and derived the proton rejection power in the following.

1. The shower starting point selection:

   Since the events with the shower starting point deeper than a lead thickness of 1 r.l. are easily selected using the imaging analysis, we selected the events which have the shower starting point smaller than 1 r.l. depth. Although almost electron events are selected, proton events are rejected down to ∼ 1/20. This proton rejection power thus becomes ∼20.

2. Discrimination with lower and upper threshold levels of the energy deposits in each BGO layer:

   As shown in Fig.1, the electron events smoothly attenuate after the shower maximum. On the other hand, the proton events do not attenuate after the shower maximum due to the successive interactions of secondary hadrons. Figure 2 shows the distribution of the energy depositions in BGO logs, converted to number of minimum ionizing particles, at each depth for 10 TeV elec-
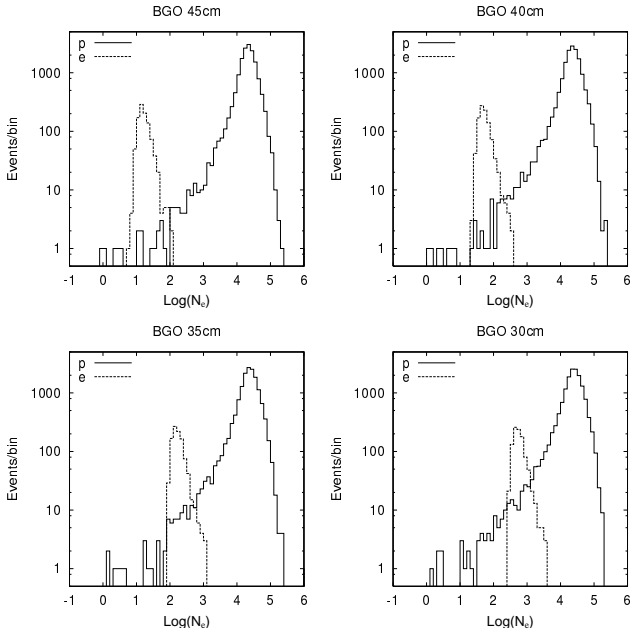
Fig. 2. Distribution of the energy depositions in 2.5 cm (2.23 r.l.) thick BGO, converted to number of minimum ionizing particles(N_e), at each depth for 10 TeV electrons (broken line) and for 30 TeV protons (solid line).

Fig. 3. Scatter plots of the energy deposition fraction of the total vs. the thickness for 10 TeV electrons (circle) and for 30 TeV protons (square) after the shower starting point selection. In the lower, the electron-like events are selected with electron surviving rate larger than 80% at 35 cm BGO thickness.

trons and 30 TeV protons. We can see that the separation between electron and proton events becomes larger as the BGO depth becomes larger. Therefore, by discriminating with lower and upper threshold levels of the energy deposition in each BGO layer, we can select the events which have electron-like development. This proton rejection method is described in details in Yoshida *et al.* (2001). Figure 3 shows an example of this selection at 35 cm BGO thickness with scatter plots of the energy depositions in each BGO layer and the observed depth. The proton rejection power of this selection for 10 TeV with electron surviving rate larger than 80% becomes 2×10^2 at 25 cm, 1×10^3 at 30 cm, 3×10^3 at 35 cm, 8×10^3 at 40 cm, and $> 2 \times 10^4$ at 45 cm BGO thickness, respectively.

3. Energy shift effect:

Since protons with energies three times larger than those of electrons are compared as the backgrounds, the number of protons at the same energy with electrons is larger by a factor of $3^{1.7}$ than the simulated number. The proton rejection power is multiplied by 6.5.

The total proton rejection power is derived from these selections. Figure 4 shows the total proton rejection power for 10 TeV with the condition of electron surviving rate larger than 80%, obtained for the different total thicknesses of BGO arrays.

With the BGO thickness of 35 cm, the total rejection power of protons can be estimated to be as large as 4×10^5

for 10 TeV in the vertical direction. At larger incident angles the rejection power should become as much as $\sim 10^6$, because the effective thickness of the calorimeter becomes larger. For example, as the effective thickness is 40 cm at an incident angle of 30 deg, the rejection power becomes larger than 10^6, as shown in Fig.4. At lower energies, the flux ratio of cosmic-ray protons to electrons is lower, and also the rejection power of protons becomes larger. As a result, we optimized the detector with the BGO thickness of 35 cm. From this optimization the size of detector was laid out to be 70cm×70cm in a restricted weight of the total payload, 2,500kg.

3.2 Electron and Gamma-ray Efficiency

Except for such hadron events as protons, gamma-ray events are also backgrounds for the electron observation. Electron has a signal in the incident position at the top layer of fibers and gamma-ray has no signals originally. However, gamma-rays have the back-scattered charged particles whose number increases more as the energy becomes higher. Since they have very similar feature of shower development with electrons, gamma-rays over 100 GeV cannot completely be rejected by such plastic scintillator as position insensitive. In the scintillating fibers, we can measure the back-scattered charged particles with a position resolution of 1 mm. In the condition of three hits (signals in three fibers) in the top four layers of scintillating fibers within 3 mm from the shower axis, the detection efficiencies of electrons and gamma-rays are larger than 95% and less than 5% for 10 GeV − 1 TeV, respectively. Conversely, this suggests that gamma-rays can be detected with such high efficiency as > 95 %, rejecting
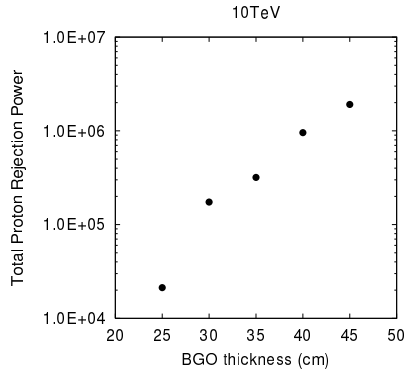
Fig. 4. The BGO calorimeter thickness dependence of the total rejection power of protons for 10 TeV with electron surviving rate larger than 80%. The incident angles are vertical.

electron events.

3.3 Energy Resolution

The energy of electro-magnetic shower is measured by the imaging sampling calorimeter and total absorption calorimeter. As a consequence of the use of a very thick calorimeter, it is easily supposed that the energy resolution can be better in higher energies. The energy resolution of electrons and gamma-rays in the energy region of $1\mathrm{GeV} - 10\mathrm{TeV}$ is represented by $30\%/\sqrt{E(\mathrm{GeV})}$, as shown in Fig.5.

In addition to the electron observation, the gamma-ray observation over the GeV region is possible by a simple improvement of the trigger system. Especially, the change of gamma-ray energy spectrum is expected in the energy region over 10 GeV for some sources. The excellent energy resolution for gamma-rays enables us to observe this spectral change.
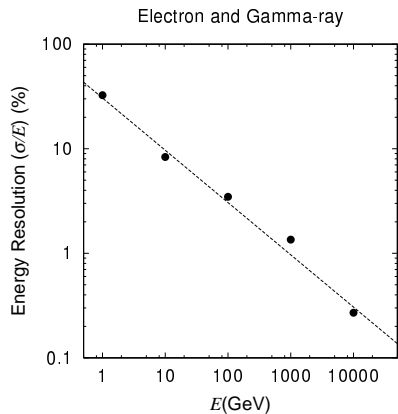
Fig. 5. Energy dependence of the energy resolution of electrons and gamma-rays. The incident angles are vertical. The errors are less than the size of symbols. The broken line shows the fitted function of $30(\%)E(\mathrm{GeV})^{-1/2}$.

Table 1. Detector Performance and Parameter.

Payload	Standard	Heavy
Energy Range(GeV)	$10-\text{several }10^3$	$10-10^4$
$S\Omega$ (m^{2}sr)	0.5	0.5$-$1.0
Proton Rejection Power	10^4	$\sim 10^6$
Energy Resolution(%)	$\sim$15	$30/\sqrt{E(\mathrm{GeV})}$
Angular Resolution(deg)	0.7$-$1.2	< 1.0
Detector Thickness(r.l.)	13	45

The detector performance and general characteristics are summarized in Table 1.

4 Summary

The preliminary simulated performance estimations given in this paper demonstrate that the CALET has a capability to observe nearly two order of magnitude more electrons above 1 TeV than the present data. In addition to the electron observation, gamma-ray observation over the GeV region is possible with excellent energy resolution.

References

Kasahara,K., *http://eweb.b6.kanagawa-u.ac.jp/~kasahara/*, 2001.

Tamura,T. *et al.*, *Adv. Space Res.*, **26**, 1397, 2000.

Torii,S. *et al.*, *Nucl. Instr. and Meth.*, **A 452**, 81, 2000.

Torii,S. *et al.*, *Astrophys. J.*, **557**, 1, 2001a.

Torii,S. *et al.*, in this volume, 2001b.

Yoshida,K. *et al.*, *Adv. Space Res.*, to be published, 2001.

Zhang,C.S., private communication, 1998.